

Utilizing Repeat UAV Imagery to Evaluate the Spatiotemporal Patterns and Environmental Drivers of Wrack in a Coastal Georgia Salt Marsh

Tyler Lynn¹ · Merryl Alber² · Jacob Shalack³ · Deepak R. Mishra¹

Received: 31 March 2023 / Revised: 10 July 2023 / Accepted: 14 August 2023 © The Author(s), under exclusive licence to Coastal and Estuarine Research Federation 2023

Abstract

Wrack, comprised of dead marsh grass, occurs naturally in salt marshes. Wrack can reduce biomass in underlying vegetation and affect salt marsh function. Unmanned aerial vehicles (UAV) provide a more efficient and cost-effective method than traditional field sampling for characterizing the distribution of wrack at a fine spatial scale. We used a DJI Matrice 210 UAV with a MicaSense Altum to collect a total of 20 images from January 2020–December 2021 in a salt marsh on Sapelo Island, GA. Wrack was classified using principal component analysis. Classified images were then used to characterize the size-frequency distribution, landscape position, and potential environmental drivers of wrack. We observed ~2100 wrack patches over the course of the study, most of which were present for only a single month. Wrack was found most frequently at the mean higher high water line (~1 m), although the areas with the highest frequency of wrack as a proportion of available marsh area were at a higher elevation (>1.3 m) and closer to creeks or shorelines (~40–50 m). High tide events were found to decrease the distance to water of wrack and increase the standard deviation of wrack elevation. This study provides a methodology for understanding wrack dynamics at a landscape scale using frequent, high-resolution UAV data.

Keywords Remote sensing · Wrack · Disturbance · Spartina alterniflora

Introduction

Salt marshes play a crucial role in the coastal landscape by providing ecosystem services such as storm protection, habitat for important fisheries, and improvements to water quality (Gedan et al. 2009; Barbier et al. 2011). They are highly productive ecosystems and play a vital role in carbon sequestration (Mitsch and Gosselink 2000; Yang et al. 2020). However, salt marshes are vulnerable to a number of naturally occurring or anthropogenic disturbances such as wrack deposition, dieback, increased nutrient loading, or human infrastructure expansion (i.e., docks or shoreline hardening)

Communicated by Brian B. Barnes

Published online: 04 September 2023

- ☑ Tyler Lynn tyler.lynn@uga.edu
- Department of Geography, University of Georgia, Athens, GA 30602-3636, USA
- Department of Marine Sciences, University of Georgia, Athens, GA 30602-3636, USA
- ³ University of Georgia Marine Institute, Sapelo Island, Athens, GA 31327, USA

(Li and Pennings 2016; Alber et al. 2008; Gilby et al. 2021; Alexander 2008).

Wrack (dead plant material) in salt marshes often floats and can be rafted around by wind, tides, or currents (Reidenbaugh and Banta 1980). Large tidal events or storm surges, taller vegetation, or localized changes in creek currents can all influence where wrack patches are deposited (Bertness and Ellison 2016; Fischer et al. 2000). Although wrack occurs naturally in salt marshes, they can affect salt marsh function and can lead to reduced biomass when deposited on vegetation (Reidenbaugh and Banta 1980; Li and Pennings 2016; Stalter et al. 2006). Longer residence times of wrack have been shown to produce greater declines in vegetation density (Stalter et al. 2006), stem density (Hanley et al. 2017), and invertebrate abundance (Hanley et al. 2017). In a study of a New England salt marsh, Bertness and Ellison (2016) found that residence times of wrack corresponded to bimonthly perigean spring tides and increased as the distance from shorelines increased, wrack distributions changed seasonally, and wrack frequently accumulated near the mean higher high water line in salt marshes. The distribution of wrack in salt marshes is also influenced by environmental factors such



as a location's elevation, distance to water, and proximity to creek bends (Bertness and Ellison 2016; Fischer et al. 2000). Fischer et al. (2000) found that areas with complex creek currents in salt marshes (i.e., creek bends or drainage channels) were most susceptible to more frequent or persistent wrack disturbances as these areas result in slower moving water that allows floating wrack to deposit on the vegetation.

The identification of wrack has historically been performed through field observations (e.g., Fischer et al. 2000; Reidenbaugh and Banta 1980; Valiela and Rietsma 1995). Field methods and monitoring can be time-intensive and/or expensive to implement (Blount et al. 2022). Previous studies that have tracked wrack in the field have been limited spatially (individual plots) and/or temporally (once or a few times a year) (e.g., Stalter et al. 2006; Valiela and Rietsma 1995; Fischer et al. 2000). Much of the previous work assessing wrack in salt marshes has placed greater emphasis on understanding the impact of wrack disturbances on vegetation using plots distributed across different marsh zones (e.g., Stalter et al. 2006; Hartman et al. 1983; Valiela and Rietsma 1995), with less emphasis on evaluating spatial patterns at landscape scales, potentially due to the difficulties (i.e., tidal limitations, inaccessibility) associated with sampling across the landscape.

There are also examples of using aerial photography to identify and analyze wrack distribution in salt marshes (e.g., Reidenbaugh and Banta 1980; Alexander 2008). These studies have shown that wrack accumulates near mean higher high water and around structures (i.e., docks) (Reidenbaugh and Banta 1980; Alexander 2008). Aerial photography, however, can be costly to implement, limiting how often or frequently imagery may be acquired for a study site (Blount et al. 2022), leaving gaps in our understanding of how wrack may be distributed at the landscape scale.

Recent improvements in unmanned aerial vehicles (UAV) and remote sensing technology have led to UAV-borne sensing being used more frequently for monitoring salt marsh ecosystems (Doughty and Cavanaugh 2019; Dronova et al. 2021). UAVs provide a method for routine monitoring and imagery for large and inaccessible study sites (Curcio et al. 2022). UAV flight plans and designs are also flexible and can be adjusted to study specific phenomena at various temporal and spatial scales (DiGiacomo et al. 2022). Although UAVs have previously been used to track wrack on beaches (Pan et al. 2021), to our knowledge, they have not been used for synoptic studies of wrack in salt marshes.

This paper presents a methodological framework to identify wrack in a salt marsh using repeating UAV-borne sensing. We used these data to characterize the spatiotemporal patterns of wrack distribution in relation to potential environmental drivers.



Methods

In this section, we present the framework we used to characterize wrack dynamics. In Fig. 1, we provide a workflow for this framework and outline the steps that we took in image processing, wrack classification, and the spatiotemporal and statistical analyses for identifying wrack using UAV imagery.

Study Area

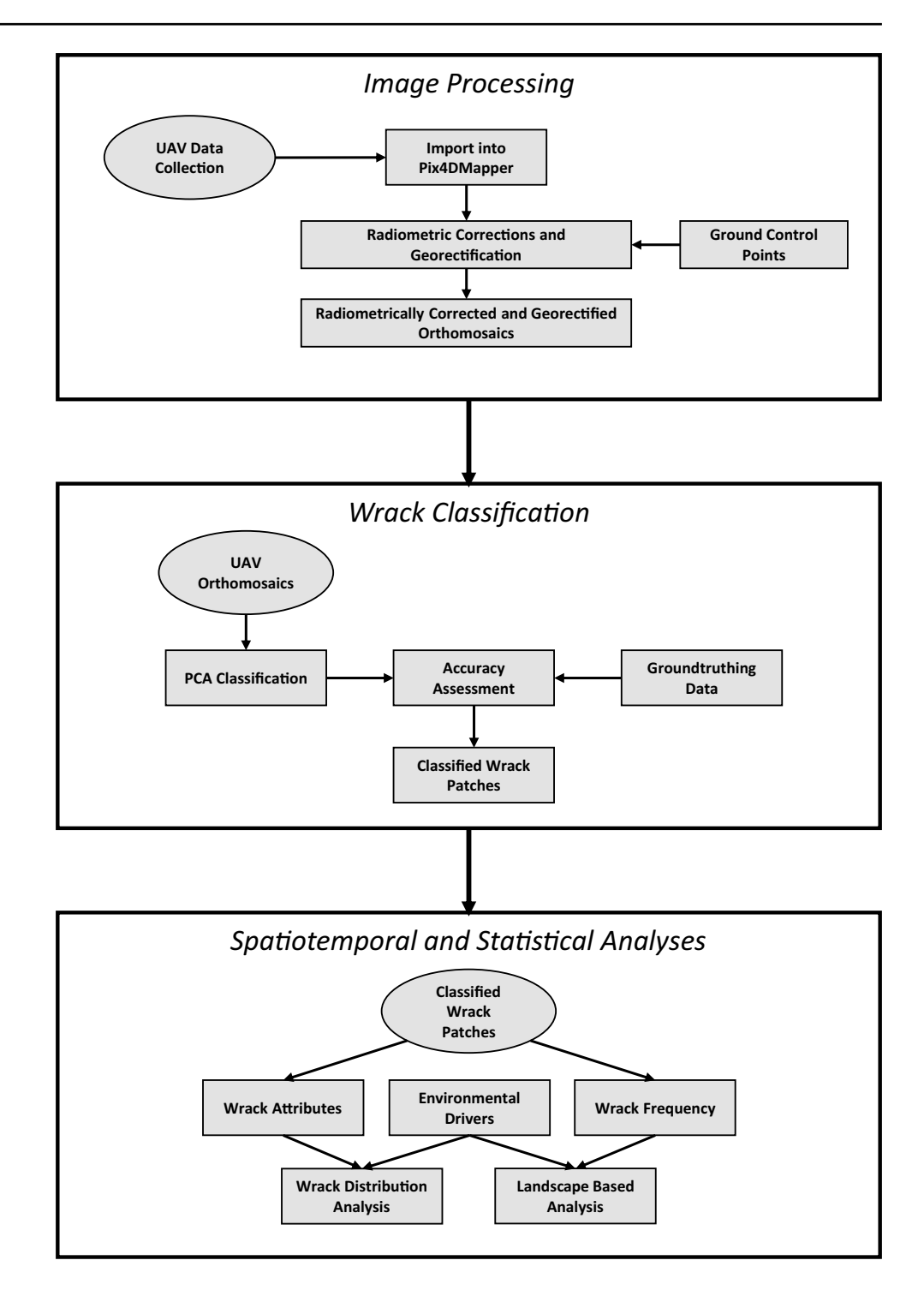
UAV imagery for this study was collected from the Dean Creek marsh on Sapelo Island, GA, a barrier island on the Atlantic US coast (Fig. 2). The 18-ha site is dominated by Spartina alterniflora and has an elevation range of 0–2 m relative to NAVD88. The site is located within the domain of the Georgia Coastal Ecosystems Long Term Ecological Research (GCE-LTER) project. The study area is also the site of ongoing research to track wrack disturbances and recovery in the field, and the results from this work support those efforts.

Data Acquisition and Pre-processing

We acquired a total of 20 aerial images of the study site from January 2020-December 2021. Eight images were acquired over the course of 2020 and 12 (monthly) images in 2021. We used a MicaSense Altum camera (MicaSense, Seattle, WA, USA) mounted on a DJI Matrice 210 UAV (DJI, Shenzhen, China). The MicaSense Altum has five multispectral bands (blue, green, red, red-edge, and nearinfrared) and one thermal infrared band. To minimize the effects of marsh inundation and sunglint, we collected data during morning low tides within 1-2 h of solar noon. Data were collected at an altitude of 120 m (resulting in a ground sampling distance of ~ 5 cm), with 80% front and side overlap, at a camera angle of 90° (nadir), and with a parallel north and south flight pattern. Pix4Dcapture (Pix4D S.A., Switzerland) and DJI Ground Station Pro (DJI, Shenzhen, China) software were both used for planning flight missions. All images were then processed using Pix4Dmapper software as described below.

Prior to each UAV flight, we used the MicaSense Altum camera to capture the calibrated RP04 reflectance panel (52.5% reflectance) supplied by MicaSense. These images were later used in Pix4Dmapper to conduct radiometric corrections during processing. The reflectance panel was selected for each band in the Pix4Dmapper software, and the reflectance factor and correction type were adjusted for the MicaSense Altum using the built-in correction factors in the Pix4Dmapper software (selected during the pre-processing

Fig. 1 Framework used in this study for processing UAV imagery, classifying wrack patches in the imagery, and the spatiotemporal and statistical analyses conducted on the classified data



steps). The MicaSense Altum Downwelling Light Sensor 2 (DLS 2) was also mounted on the UAV during flights. The DLS 2 assisted in correcting for in-flight lighting changes (i.e., cloud cover changes) in images by measuring ambient light conditions and GPS locations during the flight, which were then recorded in the image metadata and used in Pix4Dmapper software for radiometric corrections.

Twelve permanent ground control points (GCPs) were distributed ~ 100 m apart across the study area. The

number of GCPs was based on the review of recommendations from Pix4D. GCP locations were chosen in an effort to provide sufficient coverage for anticipated flight lines and boundaries of the study area. GCPs were georeferenced using a real-time kinematic global positioning system RTK-GPS (Trimble TSC7 controller and Trimble R12 GPS receiver) with a horizontal accuracy of 2.5 cm and vertical accuracy of 2 cm. These locations were surveyed before the initial flight, and the coordinates were



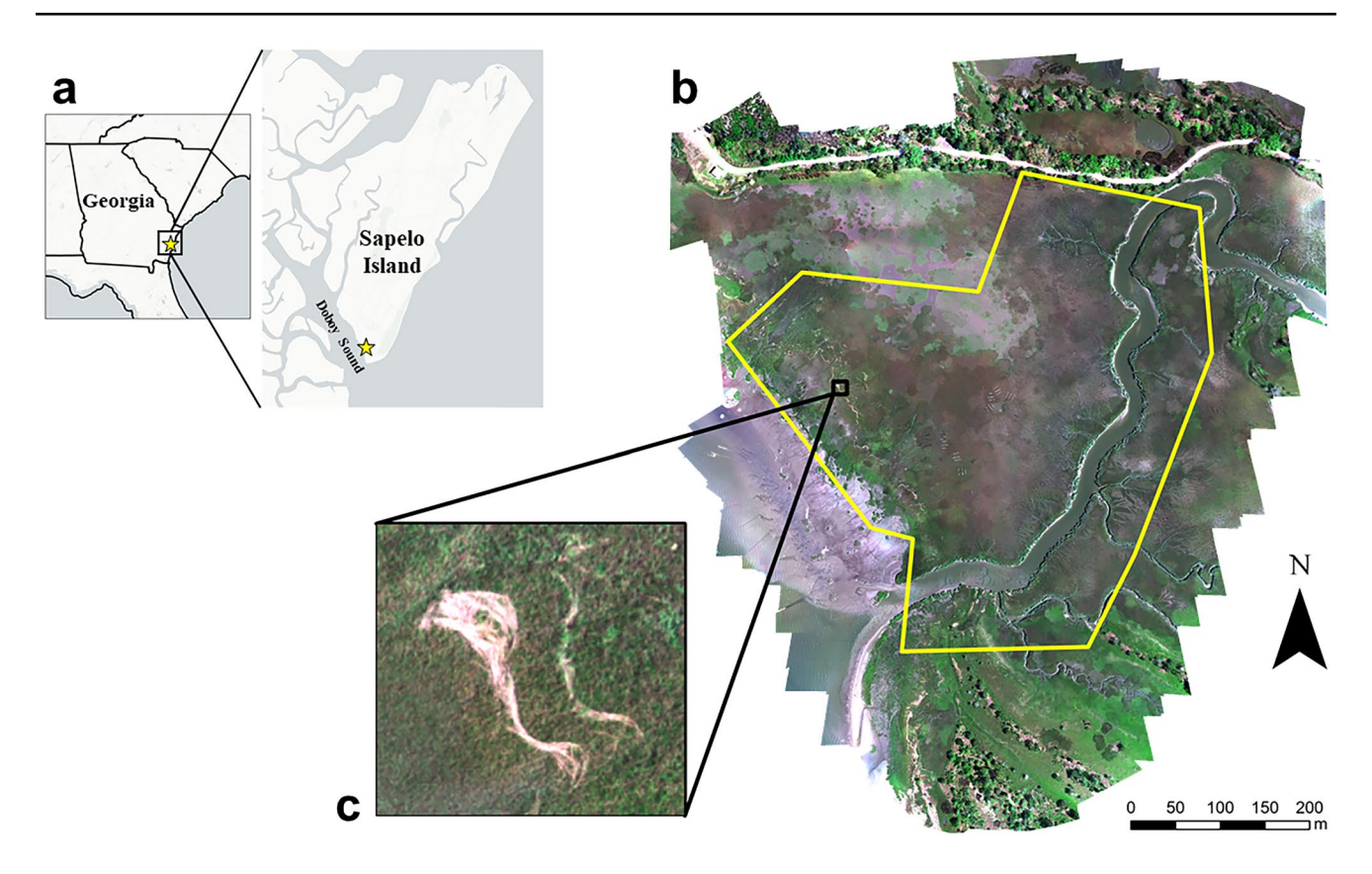


Fig. 2 Dean Creek marsh location on Sapelo Island, GA (a). Example of a UAV true color image from April 2021 with the study area polygon, which is dominated by *Spartina alterniflora*, outlined in yellow (b). Detail of a wrack package (c)

used as a reference for the georectification of all flights. Georectification was conducted in Pix4Dmapper with GCP target centers marked for different bands (~ 8–12 marks for each observation date) before proceeding with additional processing steps. Georectification of the points resulted in an average root mean square error ranging from 1–2 pixels (5–10 cm). Following radiometric corrections and georectification, data were further resampled and aligned (georegistered) to the initial UAV image (January 2020) to ensure that pixels were of a consistent, uniform size (5 cm × 5 cm) and pixel boundaries were aligned among images.

The resulting radiometric, georectified, and pixelaligned images were used as inputs in a principal component analysis (PCA) that was used to detect and identify wrack areas in the imagery (Dharani and Sreenivasulu 2021; Somayajula et al. 2021). We used the PCA tool in ArcPy to generate a PCA for each image using the multispectral bands for that image as an input. Two out of five possible PCA components from each image were selected where wrack exhibited distinct grayscale values from other features in the landscape. The PCA components we selected were not consistent throughout the study period and thus were selected through visual analysis of each component based on the histogram values of wrack in the component's metadata. A threshold was set for each selected component to distinguish between wrack and non-wrack (e.g., everything below 0.5 was considered wrack and everything above as non-wrack). Pixels that were classified as wrack in both PCA components were then classified as wrack in a binary wrack map. We used a 5×5 median filter (NumPy Python 3.7.10) on the binary wrack raster to eliminate the salt and pepper noise. The binary wrack raster was then used to create polygons of wrack packages in each scene.

To calculate the PCA classification accuracy, we randomly placed 100 points (50 wrack and 50 non-wrack areas) in the classified image and confirmed the classification through visual inspection of the true color UAV imagery. Groundtruthing points were also collected in September 2020, by visiting 60 GPS points in the study area that were randomly distributed among areas classified as wrack and non-wrack in the classified image. We used these points to confirm areas of wrack, and non-wrack could be confidently identified in UAV imagery. Classification accuracies were conducted for the first calendar year of data (8 images) to validate proof of concept for the PCA classifications.



Wrack Dynamics and Environmental Drivers

In this section, we outline the process we used to investigate the spatial patterns of wrack patches and how their abundance and temporal distribution varied. We then related this to environmental drivers to see how they influenced these patterns.

Wrack was analyzed at the polygon level to understand patterns in the area and amount of wrack patches over the course of the study. The area of each polygon was calculated using the calculate geometry function in ArcPro 2.8.0. We only considered polygons greater than 1 m² as this provides a conservative size estimate for wrack patches that are clearly detectable using UAV imagery and are large enough to affect the marsh. The area and number of wrack polygons were recorded for each image and then used to evaluate the size-frequency distributions of wrack over the study period.

We analyzed wrack characteristics, focusing specifically on wrack patch elevation, distance to water, patch area, number of patches, and total patch area for each image. We acquired 1 m elevation data from the National Elevation Dataset (NED) 3 (1/9 arc-second approximately 3 m; vertical accuracy of 2–3 m). We found that NED elevation values were within 0.2 m of RTK-GPS elevations that were collected for GCPs at our study site. NED data were resampled to match the spatial resolution of the UAV imagery (5 cm), and each wrack patch was assigned a NED value based on the average elevation of pixels within the polygon. To get a distance-to-water value for each patch, we digitized shorelines and creeks using the UAV imagery as a reference. We used the center point of each patch to calculate the Euclidean distance between a patch and the nearest creek or shoreline using the Near tool in ArcPro 2.8.0. We calculated the mean, median, standard deviation, kurtosis, and skewness of wrack patches' elevation, distance to water, and patch area of all wrack patches for each image.

We evaluated wrack characteristics in relation to three environmental drivers: tide height, wind speed, and wind direction. Tide height was calculated as the maximum tide height during the 30 days prior to each UAV image date based on the verified NOAA tidal station data product (Ft. Pulaski, Station 8670870; https://tidesandcurrents.noaa. gov). Wind speed and wind direction were acquired from the Marsh Landing weather station, which is located near the study site (Marsh Landing weather station: https://gce-lter. marsci.uga.edu/public/research/mon/marsh_landing.htm). These data were averaged for the 30 days prior to the UAV image dates. We calculated the correlation coefficients and p-values for the environmental variables (tide height, wind speed, and wind direction) and the wrack characteristics (Table S1). We selected environmental variables that were found to be significantly correlated with wrack characteristics and used linear regression to analyze the relationship.

Landscape-Based Analyses

In the previous section, we focused on the variation in wrack characteristics spatially and temporally. This section focuses on how wrack affects the broader landscape in the context of the study area. In addition, we investigate how environmental drivers further influence the distribution of wrack across the landscape.

We quantified the frequency that each location in the marsh experienced wrack to provide an understanding of the spatial distribution of wrack at the landscape scale. We used pixels rather than wrack polygons for this analysis because the polygons often change shape or move from image to image. All classified wrack rasters were added together using the Sum Raster tool in ArcPro 2.8.0. The pixel value in this raster represented the wrack accumulation frequency for that pixel over the study period. This allowed us to evaluate the cumulative distribution of wrack over the course of the study and to determine how many months each pixel was exposed to wrack.

To better understand how wrack pixels were distributed across the study site, each pixel was also assigned an elevation and distance-to-water value based on the NED data and distance measurements described in the "Wrack Dynamics and Environmental Drivers" section. We binned the data into elevation and distance intervals and then evaluated the presence of wrack in both absolute terms (the number of wrack pixels present in each bin) and as a relative proportion (the number of wrack pixels in a given bin divided by the total number of marsh pixels in that bin). We repeated the analyses on pixels that had wrack in more than one image to see if the distribution of the absolute and relative amounts of wrack changed.

Results

Wrack Identification

Wrack was readily apparent in the imagery and tended to be distributed linearly, parallel to the shoreline of Doboy Sound (Fig. 2). The overall accuracies of the PCA classifications of wrack ranged from 85 to 95%. PCA component 2 (eigenvalues ranged from 0.0002–822,345) was the most useful for identifying wrack and was most often used followed by components 4 (eigenvalues ranged from 0.00003–173,438) and 1 (eigenvalues ranged from 94,403,915–123,618,216). The green, red-edge, and near-infrared bands had the highest factor loadings from wrack pixels indicating their high importance in classifying wrack packets.



Wrack Dynamics and Environmental Drivers

We observed ~ 2100 wrack patches over the course of the study. However, both the number and area of wrack patches varied considerably from image to image. The total number of wrack patches ranged from 15 to 214 (Fig. 3a), and the cumulative area of patches ranged from 140 to 1081 m^2 (Fig. 3b). Both the greatest number of wrack patches and highest total wrack area were observed in November 2021. There were also smaller peaks in the total wrack area observed in August 2020 and 2021. The lowest number of patches was observed in October 2020, and the lowest cumulative area of patches was observed in January 2020.

The number of wrack patches showed a consistent lognormal distribution throughout the study period (Fig. 4a), with the greatest number of wrack patches in the smallest size class $(1-5 \text{ m}^2)$. In contrast, the area of wrack patches had a bimodal distribution pattern (Fig. 4b), with the largest peak in the smallest size class $(1-5 \text{ m}^2)$ and a smaller peak for patches with a size between 25 and 100 m. The largest wrack patch we observed, in July 2020, was 278 m².

We tried all possible variations, and out of the three environmental variables we tested, maximum tide height from the 30 days prior to UAV observations was the only one that was significantly correlated with wrack characteristics. Maximum tide height was significantly correlated with both the median distance to water of the wrack patches ($R^2 = 0.57$, p-value < 0.001) (Fig. 5a) and the standard deviation of wrack elevation ($R^2 = 0.32$, p-value = 0.009) (Fig. 5b). Tide height, wind speed, and wind direction were not significantly correlated with other statistical measurements of wrack patch characteristics that we tested (Table S1).

Fig. 3 Total number (a) and area (b) of wrack patches observed within the study area between January 2020 and December 2021. Each point represents a UAV image with gaps in the series indicating times when the UAV was not operational. The highest number and area of wrack patches were both observed in November 2021 following a high tide event

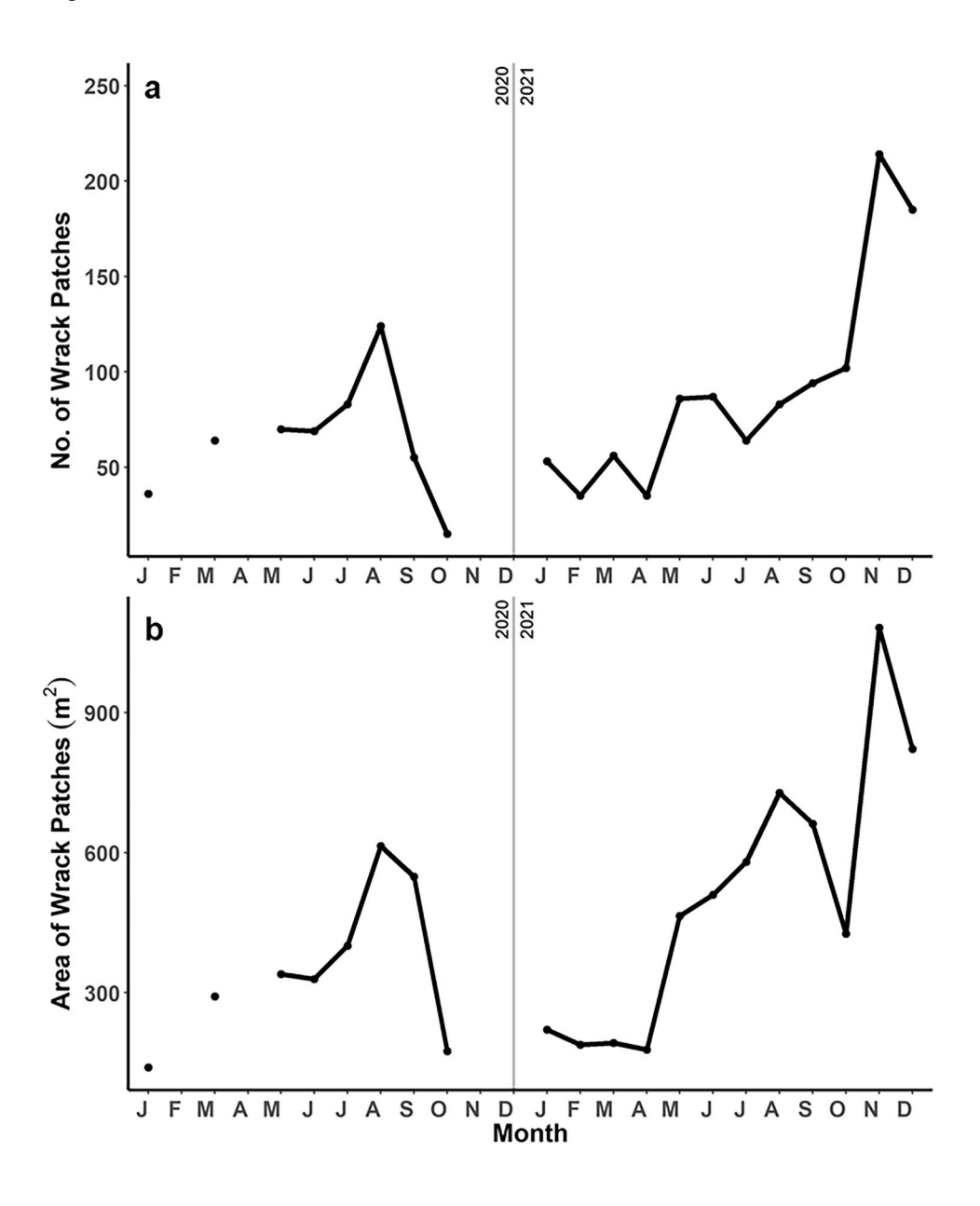
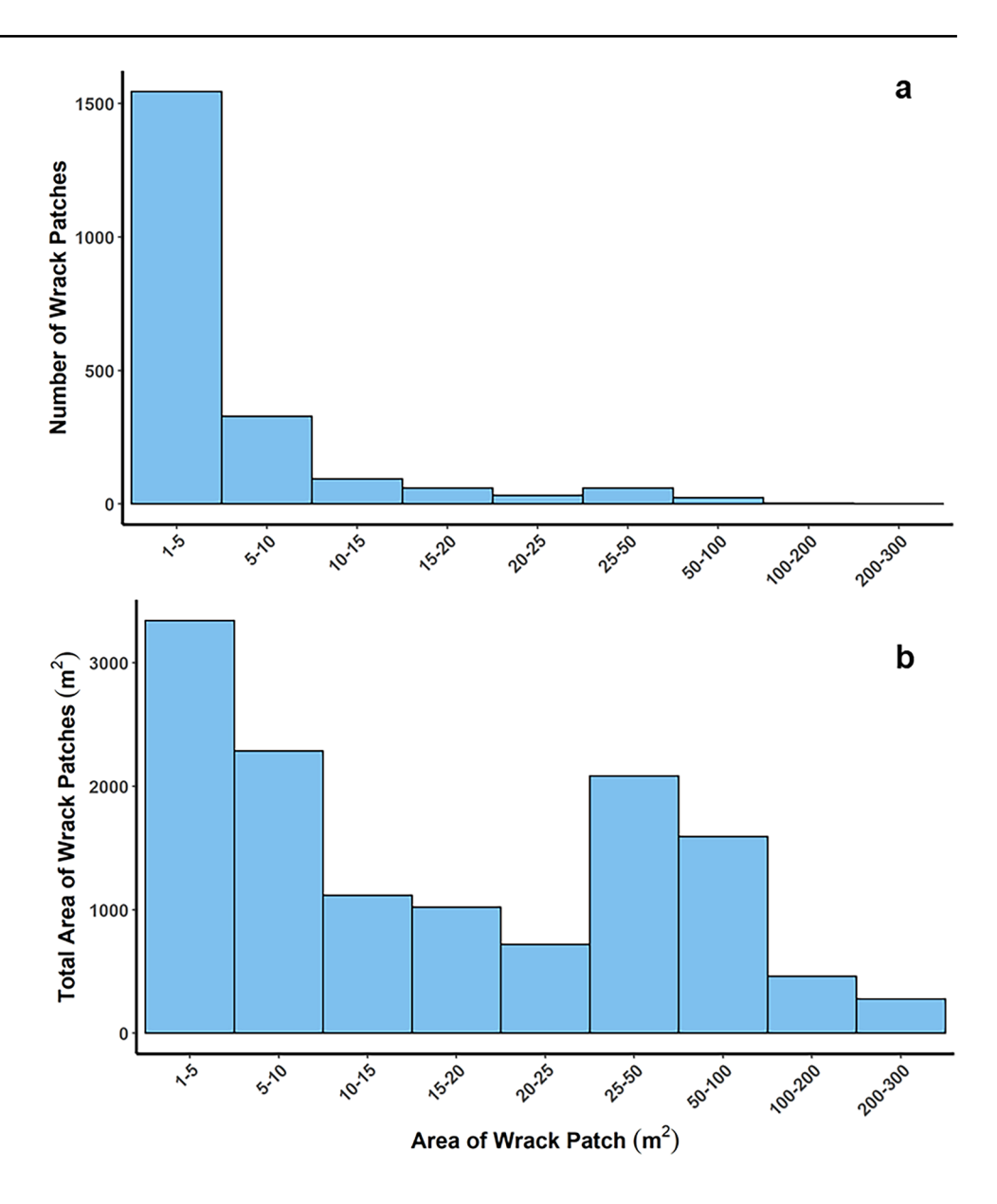




Fig. 4 Size-frequency distribution of the number of wrack patches (a) and wrack patch area (b) observed in the study area over the entire study period between January 2020 and December 2021 (20 UAV images). Patches were grouped in bins according to their area (the range of each bin is indicated in meters)



Landscape-Based Analyses and Environmental Drivers

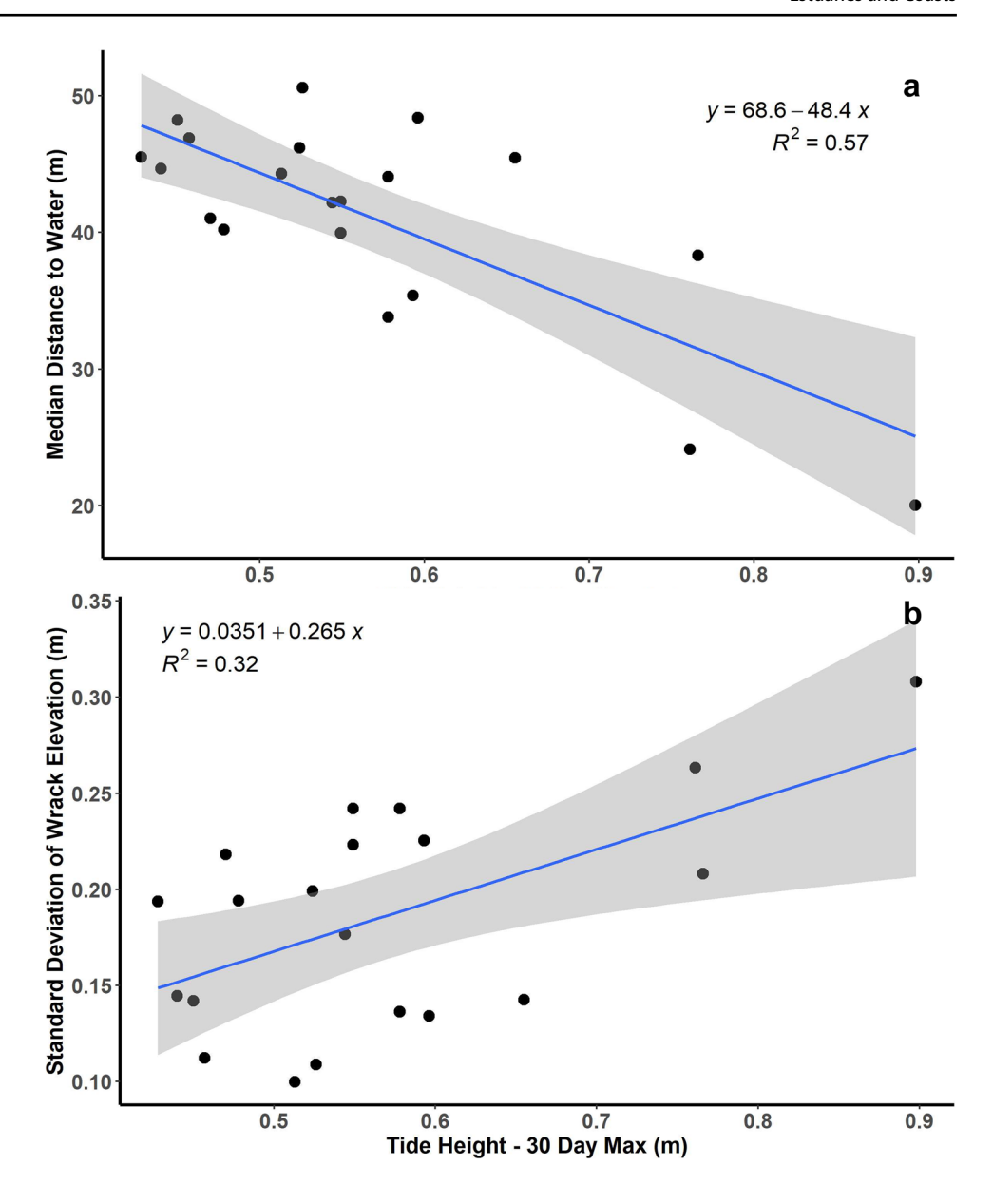
We used the pixel data to identify the frequency with which wrack affected each part of the marsh. Although wrack was present in all images, wrack pixels covered only 2% of the study area over the entire course of the study (Fig. 6). Fifty-eight percent of the wrack-affected pixels had wrack for only a single observation, and 90% of the pixels had wrack for less than four observations (Table 1). The highest number of repeated observations of wrack was in 11 images (out of 20), which occurred in 500 pixels.

We binned wrack pixels by elevation and distance to water to analyze the occurrence of wrack across the marsh landscape. Pixels with wrack were most frequently observed in areas near mean higher high water (~ 1 m elevation) and within 50–75 m from the nearest creekbank or shoreline

(Fig. 7a). Sixty percent of the pixels in the study area have an elevation of ~ 1 m, and these areas also had the highest total number of pixels with wrack. We normalized the distribution of wrack pixels (number of pixels with wrack divided by the proportion of pixels in individual bins) to identify areas of higher wrack frequency relative to the number of marsh pixels in the study area. High elevation areas (> 1.3 m) and areas between 10 and 40 m from water were disproportionally affected by wrack (~ 80% of pixels in these areas had wrack). In contrast, where wrack occurred most frequently (1–1.1 m in elevation and 50–60 m from water), only 30% of the possible pixels in that bin were affected (Fig. 7b). When we confined our analysis to pixels where wrack was present for more than one image, the bins with the highest amount of wrack were the same in both absolute and relative distribution (Fig. 7c, d).



Fig. 5 Relationship between the maximum tide height of the previous 30 days (x-axis) and a median distance to water of wrack patches (y-axis) and b standard deviation of elevation of wrack patches (y-axis) observed within each UAV image used in the study. Solid lines show the linear fit, and gray shaded areas represent the 95% confidence interval (equations as shown)



Discussion

The methodology presented in this paper provides a framework for identifying the spatial and temporal patterns of wrack using multispectral UAV data. Although aerial photography (e.g., Reidenbaugh and Banta 1980; Alexander 2008) has been used previously to evaluate wrack distribution, these studies were limited to 1–3 images per year and had coarse spatial resolutions. Our study improves on this with consistent UAV imagery collection and further demonstrates how this emerging technology may be useful for wetland researchers to establish high spatial resolution data, with consistent frequency at the landscape scale. We collected 20 images over the course of 2 years, which allowed us to characterize wrack patches and evaluate how wrack distribution patterns change both spatially and temporally.

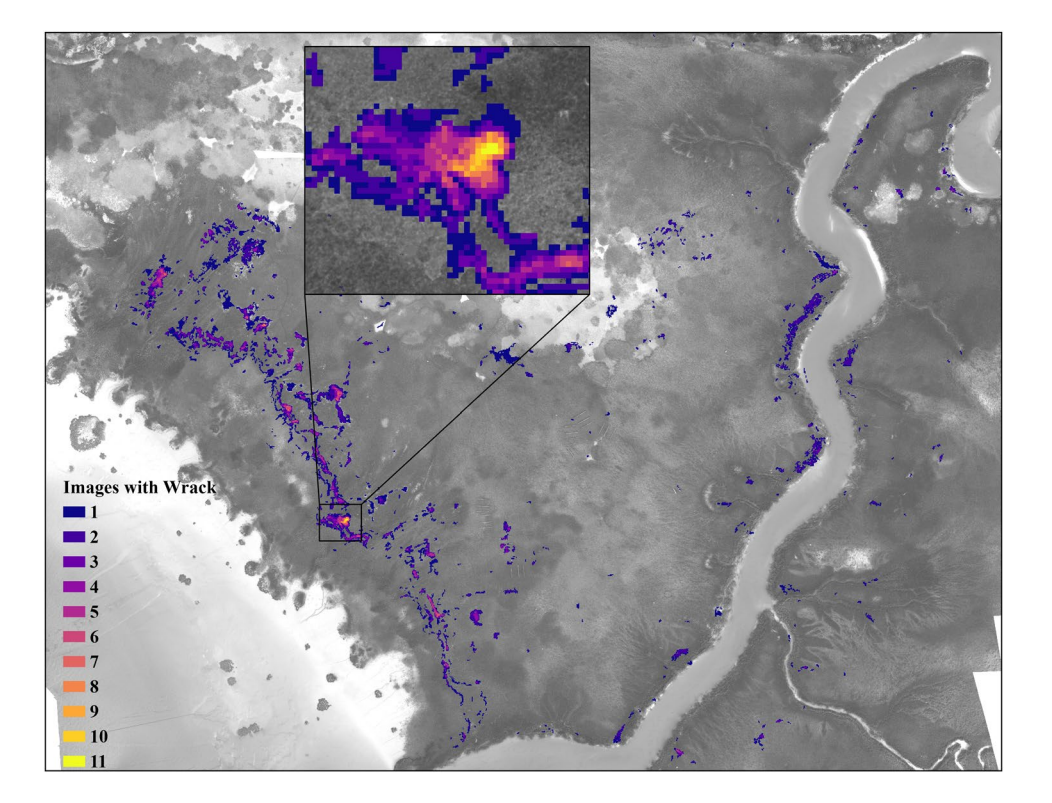
Wrack Identification

The PCA classification method resulted in a high accuracy (between 85 and 95% overall accuracy) classification of wrack. Although other classification methods are readily available, the PCA classification could be conducted with limited ground data and did not require extensive training of the very large UAV files (several GBs). An additional motivation of this study was to identify wrack patches for sampling by a field crew, and PCA allowed us to quickly identify wrack patches that could be targeted for field sampling immediately following the UAV flight.

PCA components 2, 4, and 1 were used most frequently for classifying wrack, and the factor loadings for these bands indicated that the green, red-edge, and near-infrared bands provided the most information for these components. The



Fig. 6 Grayscale image with pixels highlighted based on the number of times wrack was observed in UAV images over the course of the study. Shades range from dark purple (1 UAV image with wrack) to yellow (11 UAV images with wrack). The inset shows an example of the variation in wrack frequency that can be present within a small area



importance of these bands for classifying wrack can be explained by how they interact spectrally with wrack and other features in the study site.

Wrack patches generally had higher reflectance values in the visible spectrum (465–722 nm). We saw this in a visual inspection of RGB images and when analyzing the individual remote sensing bands (where wrack appeared as brighter shades of gray). Green wavelengths (550–570 nm) were reflected by both wrack and vegetation. Red-edge (712-722 nm) wavelengths were also reflected by wrack, whereas vegetation absorbed light in these wavelengths. Wrack reflected lower amounts of NIR (820-860 nm), and healthy vegetation in the study area reflected high amounts of NIR light. Mudflats, which behaved similarly to wrack in the visible spectrum, had lower NIR reflectance values than wrack (Huete 2004; Munyati 2004). Other bands may not have been as important in the PCA due to mixed reflectance signals from vegetation growing through wrack patches, sparse wrack patches where the signal from wrack

Table 1 Total number of pixels that were classified as wrack in all images separated by the number of UAV images where that pixel had wrack. The corresponding area of wrack that was classified as wrack

and surrounding vegetation may have been mixed, or pixels on the edges of wrack patches which would include a signal from wrack and healthy vegetation.

Wrack Dynamics and Environmental Drivers

Most of the wrack patches that we observed were smaller in area, with the majority of the wrack patches between 1 and 5 m². Patches between 1 and 5 m² also had the largest overall contribution to the total amount of wrack observed over the study period. However, there were still several wrack patches that were over 25 m². These results are similar to findings from Valiela and Rietsma (1995) where the majority of the wrack patches that were identified were between 1 and 100 m². We did not specifically analyze wrack duration; however, visible inspection of our wrack frequency analyses showed that larger patches of wrack tended to stay in place for longer than 4 months. Large wrack mats have been shown to be more likely

is shown in the bottom row. These observations cover the entire study period between January 2020 and December 2021. No pixel had wrack in more than 11 of the 20 UAV images

# of Images	1	2	3	4	5	6	7	8	9	10	11
# of Pixels	1190000	513100	151700	93000	44500	20000	6100	1800	1800	700	500
Area (m²)	2975	1283	379	233	111	50	15	5	5	2	1



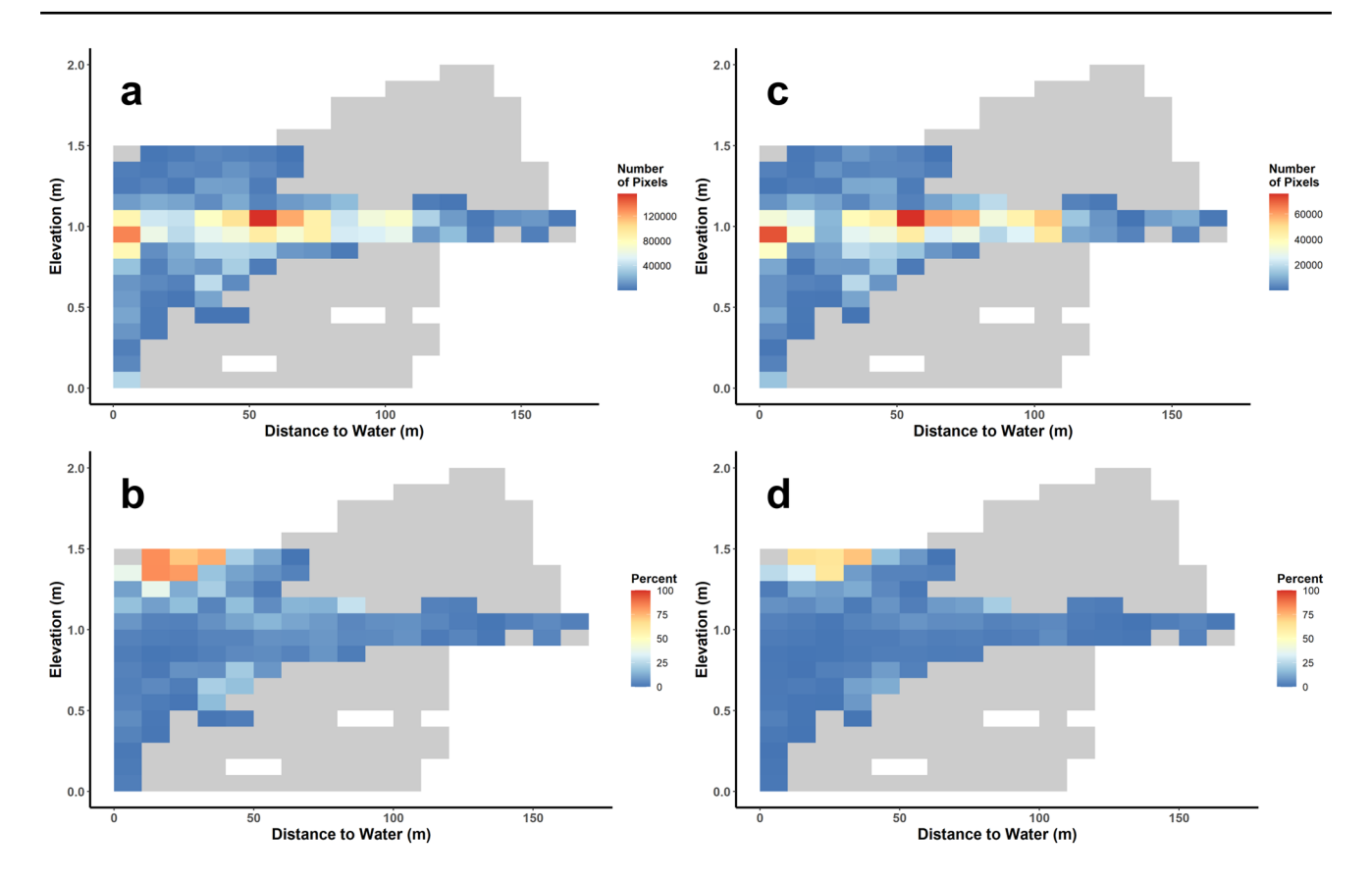


Fig. 7 Absolute (\mathbf{a}, \mathbf{c}) and relative (\mathbf{b}, \mathbf{d}) number of pixels with wrack observed in the study area grouped into bins of elevation and distance to water. In \mathbf{a} and \mathbf{c} , shading represents the total number of pixels with wrack that were observed in each bin. In \mathbf{b} and \mathbf{d} , shading represents the number of pixels with wrack as a percentage of the total number of available pixels within a given bin. \mathbf{a} and \mathbf{b} tally pixels that had wrack in at least one image, whereas \mathbf{c} and \mathbf{d} only include

pixels that had wrack in more than one image. In all figures, gray areas are bin combinations within the study area where wrack was never observed, and blank areas are bin combinations that were not represented in the study area. These data are based on all 20 of the UAV images taken within the study area between January 2020 and December 2021

to damage vegetation (Valiela and Rietsma 1995), and future work should analyze how wrack size may influence wrack duration.

In our study, wrack abundance had peaks in August of both years and November 2021. The peaks in the wrack area that we observed in August of 2020 and 2021 were both followed by similar declines in the wrack area in September and October. The peak we observed in November 2021 was associated with a high tide event that occurred 8 days prior to the UAV flight. This peak may also be seasonal as we might expect more wrack following plant senescence in the fall. However, Bertness and Ellison (2016) noted a peak in wrack in summer in Rhode Island, whereas Valiela and Rietsma (1995) noted a peak in spring in MA, suggesting that factors beyond the season, such as variation in tidal cycles and wind events, are also likely important.

We found that tide height was negatively related to the distance of wrack patches from the water and positively related to the standard deviation of wrack elevation. This is surprising, as the increased energy and inundation of the higher tides serve to lift the wrack and keep it suspended for longer than occurs during lower tides. During the ebb tide, however, we speculate that the wrack gets caught by the high vegetation that borders the creek. It may also be that some of the material is deposited higher at the upland edge of the marsh by the flood tide, which is beyond the scope of this study as we were focused on the portion of the marsh that is dominated by Spartina. In both instances, the higher tides may lead to wrack being deposited along the entire elevation gradient during the ebb tide, thus increasing the overall distance of wrack patches from the water and the standard deviation of wrack elevation. These findings are consistent with those of previous studies that have shown that tide height affects wrack movement and that wrack abundance is highest at lower elevations (Reidenbaugh and Banta 1980; Bertness and Ellison 2016).

Previous studies have speculated that wind (through field observations; Reidenbaugh and Banta 1980) may influence wrack deposition in salt marshes. Although we found that wind speed and wind direction were negatively correlated



with wrack patches' distance to water, these relationships were not significant (Table S1). This may be partially attributed to the fact that we characterized wrack over intervals of a month or more, as opposed to daily, and then compared that to median and mean wind speeds and directions for the prior 30 days before the UAV flight. The effects of wind speed and direction may be lost when averaged over the course of an entire month.

Landscape-Based Analysis and Environmental Drivers

Our observations of wrack pixels show that only a small portion (< 1%) of the study area may have wrack at any given time, most areas only have wrack for a single image, and only a small portion (~ 2%) of the study area was impacted by wrack throughout the course of the study. Moreover, most of the wrack we observed stayed for 3 months or less. Valiela and Rietsma (1995) found most wrack patches to stay for either a single month or for 3–4 months with most patches (70%) resulting in no damage to vegetation. Previous studies of wrack disturbance have shown that measurable declines in vegetation and biomass start to occur after two consecutive months (Bertness and Ellison 2016; Reidenbaugh and Banta 1980; Stalter et al. 2006). This may suggest that most of the wrack observed in our study may not result in a disturbance as 90% of the wrack pixels did not have wrack for longer than 3 months, with the majority only present at a location for a single month. However, there were still 10% of the wrack pixels that were covered for more than 3 months, and we would expect a greater impact on vegetation and biomass in these locations.

We observed the highest frequency of wrack at elevations between 0.9 and 1.1 m and 50 m from water. This elevation roughly corresponded with the mean higher high water for our study site. The highest relative proportion of wrack was seen in areas of high elevation (> 1.3 m) and near creeks or shorelines (50-75 m) suggesting that these areas may be particularly vulnerable to wrack disturbances. Wrack that accumulated in these areas did not appear to be associated with any particular tidal event. However, in our observations, wrack did tend to stay in these areas for more than a single month. Our findings match previous studies that have seen the highest accumulation of wrack at the mean higher high water line in salt marshes (Bertness and Ellison 2016; Valiela and Rietsma 1995). Although the distance where wrack accumulated most frequently varied (5-75 m from shorelines in this study vs. 8-10 m in Bertness and Ellison 2016), this distance was associated with mean higher high water at both sites.

Our analyses of wrack dynamics indicate that most wrack patches are short-lived (1 month) and accumulate most frequently at high tidal lines or near creeks. High tide events also influence wrack deposition, decreasing the distance of wrack patches to water and increasing the overall elevation range of wrack patches. Wrack patches occurred most frequently at mean higher high water and were often distributed at tidal lines parallel to the Doboy Sound. However, we saw the greatest proportion of wrack at higher elevations that were near water. These results provide a baseline for understanding wrack effects on marshes and identifying areas that may be most vulnerable to wrack disturbances.

Supplementary Information The online version contains supplementary material available at https://doi.org/10.1007/s12237-023-01265-z.

Acknowledgements We thank Wade Sheldon, Adam Sapp, Dontrece Smith, Elise Diehl, and John Williams for their assistance in collecting and managing data, and the GCE Disturbance working group for their feedback and guidance in developing this manuscript. This is contribution 1116 of the University of Georgia Marine Institute.

Funding The Georgia Coastal Ecosystems Long Term Ecological Research is supported by the National Science Foundation funding (OCE-1832178).

Data Availability Data that support the findings of this study are openly available in the GCE-LTER Data Catalog: Wrack classification data based on UAV imagery from Dean Creek on Sapelo Island, GA: http://dx.doi.org/10.6073/pasta/964d3375e5bbc81847fa72093bb087ef

Declarations

Competing Interests The authors declare no competing interests.

References

Alber, M., E.M. Swenson, S.C. Adamowicz, and I.A. Mendelssohn. 2008. Salt marsh dieback: An overview of recent events in the US. Estuarine, Coastal and Shelf Science 80 (1): 1–11. https://doi.org/ 10.1016/j.ecss.2008.08.009.

Alexander, C. 2008. Wrack assessment using aerial photography in Coastal Georgia. (April).

Barbier, E.B., D.H. Sally, K. Chris, W.K. Evamaria, C.S. Adrian, and R.S. Brian. 2011. The value of estuarine and coastal ecosystem services. *Ecological Monographs* 81 (2): 169–193. https://doi.org/10.1890/10-1510.1.

Bertness, M.D., and A.M. Ellison. 2016. Determinants of pattern in a New England salt marsh plant community. *Ecological Monographs* 57 (2): 129–147.

Blount, T.R., A.R. Carrasco, S. Cristina, and S. Silvestri. 2022. Exploring open-source multispectral satellite remote sensing as a tool to map long-term evolution of salt marsh shorelines. *Estuarine, Coastal and Shelf Science*, 266 (November 2021).https://doi.org/10.1016/j.ecss.2021.107664.

Curcio, A.C., G. Peralta, M. Aranda, L. Barbero. 2022. Evaluating the performance of high spatial resolution UAV-photogrammetry and UAV-LiDAR for salt marshes: the Cádiz Bay study case. *Remote Sensing*, 14 (15).https://doi.org/10.3390/rs14153582.

Dharani, M., and G. Sreenivasulu. 2021. Land use and land cover change detection by using principal component analysis and morphological operations in remote sensing applications. *International Journal of Computers and Applications* 43 (5): 462–471. https://doi.org/10.1080/1206212X.2019.1578068.



- DiGiacomo, A.E., R. Giannelli, B. Puckett, E. Smith, J.T. Ridge, and J. Davis. 2022. Considerations and tradeoffs of UAS-based coastal wetland monitoring in the Southeastern United States. Frontiers in Remote Sensing 3 (August): 1–20. https://doi.org/10.3389/frsen. 2022.924969.
- Doughty, C.L., and Cavanaugh, K.C. 2019. Mapping coastal wetland biomass from high resolution unmanned aerial vehicle (UAV) imagery. *Remote Sensing*, 11 (5). https://doi.org/10.3390/rs11050540
- Dronova, I., Kislik, C., Dinh, Z., and Kelly, M. 2021. A review of unoccupied aerial vehicle use in wetland applications: emerging opportunities in approach, technology, and data. *Drones*, 5 (2).https://doi.org/10.3390/drones5020045.
- Fischer, J.M., T. Reed-Andersen, J.L. Klug, and A.G. Chalmers. 2000. Spatial pattern of localized disturbance along a southeastern Salt Marsh tidal creek. *Estuaries* 23 (4): 565–571. https://doi.org/10.2307/1353146.
- Gedan, K.B., B.R. Silliman, and M.D. Bertness. 2009. Centuries of human-driven change in salt marsh ecosystems. *Annual Review of Marine Science* 1: 117–141. https://doi.org/10.1146/annurev.marine.010908.163930.
- Gilby, B.L., M.P. Weinstein, R. Baker, J. Cebrian, S.B. Alford, A. Chelsky, and S.L. Ziegler. 2021. Human actions alter tidal marsh seascapes and the provision of ecosystem services. *Estuaries and Coasts*, 44 (6): 1628–1636.https://doi.org/10.1007/s12237-020-00830-0.
- Hanley, T.C., D.L. Kimbro, and A.R. Hughes. 2017. Stress and subsidy effects of seagrass wrack duration, frequency, and magnitude on salt marsh community structure. *Ecology* 98 (7): 1884–1895. https://doi.org/10.1002/ecy.1862.
- Hartman, J., H. Caswell, and I. Valiela. 1983. Effects of wrack accumulation on salt marsh vegetation. Oceanologica Acta, Actes 17e, 99–102.
- Huete, A.R. (2004). Remote sensing for environmental monitoring. In Environmental Monitoring and Characterization, ed. J. F. Artiola, I. L. Pepper, M. L. Brusseau, 183–206. Academic Press.
- Li, S., and S.C. Pennings. 2016. Disturbance in Georgia salt marshes: Variation across space and time. *Ecosphere* 7 (10): 1–11. https://doi.org/10.1002/ecs2.1487.

- Mitsch, W.J., and J.G. Gosselink. 2000. Wetlands. New York: John Wiley & Sons, 3rd edition.
- Munyati, C. 2004. Use of principal component analysis (PCA) of remote sensing images in wetland change detection on the Kafue Flats. Zambia. Geocarto International 19 (3): 11–22. https://doi. org/10.1080/10106040408542313.
- Pan, Y., M. Flindt, P. Schneider-Kamp, and M. Holmer. 2021. Beach wrack mapping using unmanned aerial vehicles for coastal environmental management. *Ocean and Coastal Management*, 213 (July): 105843.https://doi.org/10.1016/j.ocecoaman.2021.105843.
- Reidenbaugh, T.G., and W.C. Banta. 1980. Origins and effects of Spartina wrack in a Virginia salt marsh. *Gulf Research Reports*, 6 (4): 393–401.https://doi.org/10.18785/grr.0604.07.
- Somayajula, V., D. Ghai, and S. Kumar. 2021. Land use / land cover change analysis using NDVI, PCA. Proceedings of the fifth international conference on computing methodologies and communication (ICCMC 2021), 849–855.
- Stalter, R., A. Jung, A. Starosta, J. Baden, and M.D. Byer. 2006. Effect of wrack accumulation on salt marsh vegetation, Baruch Institute, Georgetown County, South Carolina. WIT Transactions on Ecology and the Environment 88: 305–313. https://doi.org/10.2495/ CENV060291.
- Valiela, I., and C.S. Rietsma. 1995. International association for ecology disturbance of salt marsh vegetation by wrack mats in Great Sippewissett Marsh Published by: Springer in cooperation with International Association for Ecology Stable. *Ecology*, 102 (1): 106–112. http://www.jstor.org/stable/4220934.
- Yang, D., X.Y. Miao, B. Wang, R.P. Jiang, T. Wen, M.S. Liu, and C. Xu. 2020. System-specific complex interactions shape soil organic carbon distribution in coastal salt marshes. *International Journal of Environmental Research and Public Health*, 17 (6).https://doi.org/10.3390/ijerph17062037.

Springer Nature or its licensor (e.g. a society or other partner) holds exclusive rights to this article under a publishing agreement with the author(s) or other rightsholder(s); author self-archiving of the accepted manuscript version of this article is solely governed by the terms of such publishing agreement and applicable law.

